Electronic Supplementary Material (ESI) for Dalton Transactions.
This journal is © The Royal Society of Chemistry 2020

Supporting Information

Water Adsorption Fingerprinting of Structural Defects/Capping functions in Zr-fumarate MOFs: A Hybrid Computational-Experimental Approach

Paulo G. M. Mileo[§], Kyung Ho Cho,[†] Jong-San Chang*[,†,€] and Guillaume Maurin,*[,§]

[§] ICGM, Univ. Montpellier, CNRS, ENSCM, Montpellier, France

[†]Research Group for Nanocatalyst and Chemical Safety Research Center, Korea Research Institute of Chemical Technology (KRICT), Gajeong-ro 141, Yuseong-gu, Daejeon 34114, South Korea

[€]Department of Chemistry, Sungkyunkwan University, Suwon 440-476, South Korea

*Corresponding authors: guillaume.maurin1@umontpellier.fr, jschang@krict.re.kr

1. Molecular simulations

Defective MOF-801 structure models were created by manually selecting and removing either individual linkers (ml configurations) or inorganic clusters together with their connected linkers (mc configurations). The resulting dangling Zr bonds were then saturated by either formate or H2O/OH groups so as to generate uniform distributions of these capping agents over the MOF scaffolds. From a previous work[1] and preliminary simulations, we observed the relative disposition of these defects to play a secondary role on the adsorption properties of the resulting structure models. All the generated defective structures were geometry-optimized at the DFT level maintaining the experimental unit cell parameters fixed employing a PBE-GGA functional[2] combined with Gaussian basis sets and pseudopotentials as implemented in the CP2K package[3,4]. The triple-ζ valence plus double polarization (TZV2P) basis set[5] was used for the H, O, and C atoms, while the Zr atoms were treated using the double-ζ valence plus polarization (DZVP) basis set[6]. The pseudopotentials used for all the atoms were those derived by Goedecker, Teter and Hutter[7]. A relative cutoff of 500 Ry and a convergence criterion of 10^{-6} for the self-consistent field interactions were employed. Dispersion corrections were implemented with the use of the DFT-D3 method[8]. The partial charges of each atom type of the framework were calculated using the REPEAT method[9] and are directly reported in all cif files.

Pore size distributions (PSDs) were calculated for the non-defective structure and for the structures incorporating 4 missing linker defects (*ml_4* configuration) and 2 missing cluster defects (*mc_2* configuration). In each case, two configurations with either H_2O/OH or $HCOO^-$ terminal groups to saturate the Zr atoms were considered.

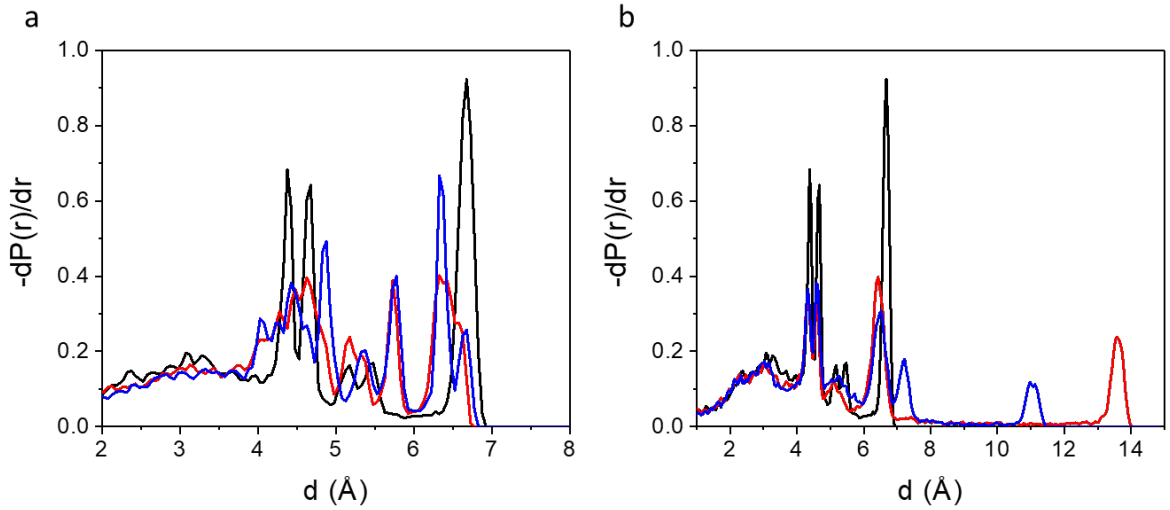

Figure S1 – PSD plots for the defective *ml₄* (a) and *mc₂* configurations (b) with H_2O/OH (red lines) and formate (blue lines) terminal groups. For comparison the PSD plot for the ideal MOF-801 structure is reported as black line,

GCMC simulations using the Complex Adsorption and Diffusion Simulation Suite (CADSS) code were carried out to predict the adsorption behaviour for the ideal and defective structure models of MOF-801 at 298 K. All these MC simulations were carried out with 2×10^8 production steps preceded by 10^7 equilibration steps in order to achieve equilibrium configurations for each point of the simulated isotherms. The simulation boxes were made of 2×2×2 unit cells for each DFT optimized defective structure, where the host atoms were kept fixed in their initial positions.The adsorption enthalpies (ΔH_{ads}) were calculated from the GCMC simulations using the revised Widom's test particle insertion method[10].

The non-bonded interactions between water molecules and the MOF framework was modelled by Coulombic and Lennard-Jones (LJ) potential terms. LJ parameters assigned to atoms of the inorganic and organic nodes were obtained from the UFF[11] and DREIDING[12] generic force fields respectively. Crossing host/guest interactions were modelled using the Lorentz-Berthelot mixing rules[13]. The short-range dispersion forces described by the LJ potential was truncated at a cut-off radius of 12 Å while the Ewald summation[14] method was

used to compute the long-range Coulombic contributions. Following the treatment adopted in other forcefields,[15,16] the interactions associated with the polar hydrogens of both terminal water molecules and OH terminal groups of MOF-801 were modelled using only electrostatic interactions. The water molecules were represented by the 4-site water model TIP4P/2005[17].

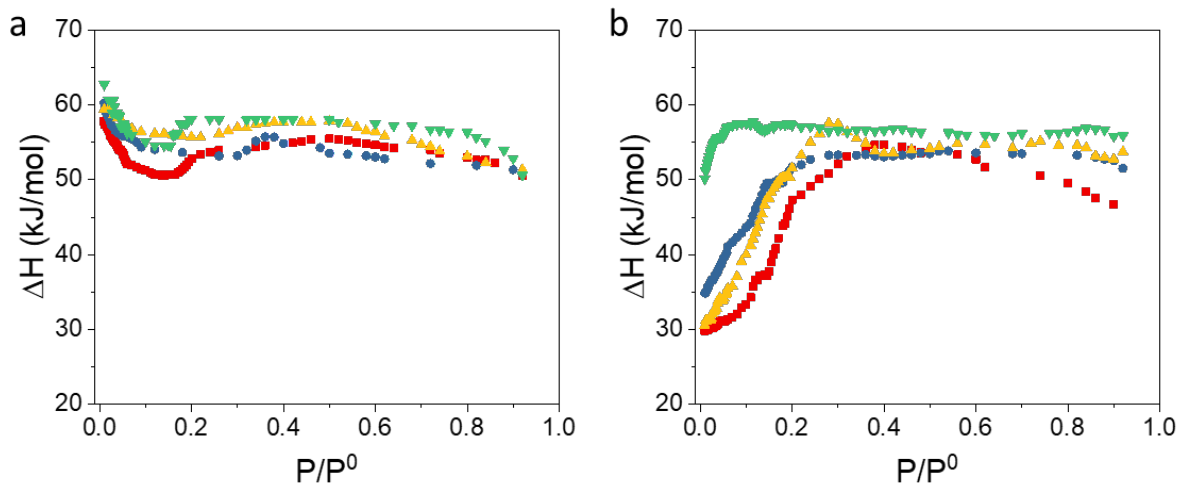

Figure S2. GCMC simulated adsorption enthalpies obtained at 298K for ml_1 (□), ml_2 (□), ml_3 (□), and ml_4 (□) configurations coordinated to H_2O/OH (a) and formate (b) groups.

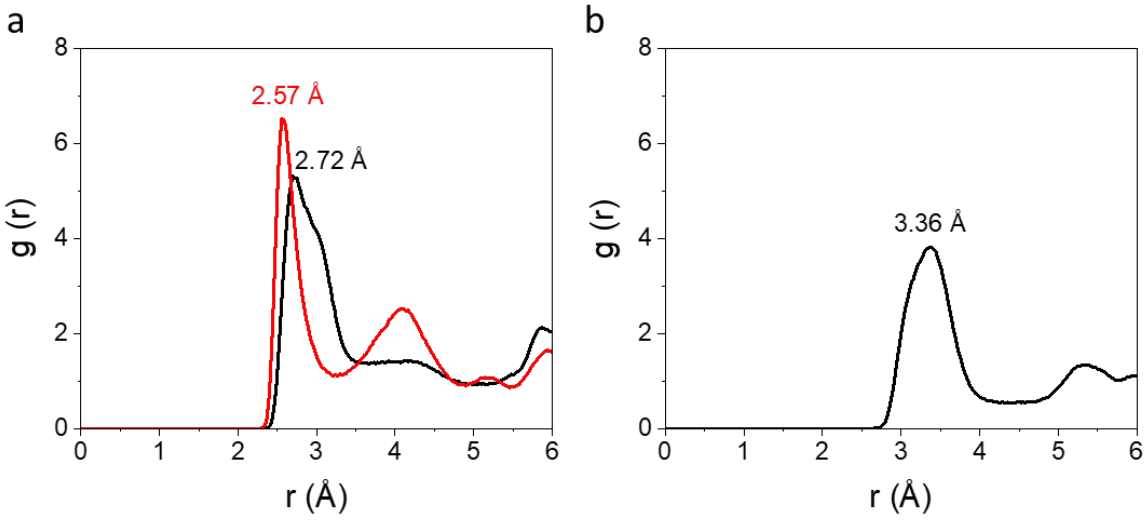

Figure S3. Selected radial distribution functions obtained from GCMC water adsorption calculations on *ml₁* defective model having OH/H_2O (a) and $CHOO^-$ (b) as capping functions. The donor-acceptor interactions between the adsorbed water molecules and O atoms of H_2O (black line)/OH (red line) terminations (a) and the C atoms of formate groups (b) are described at the initial stage of water adsorption.

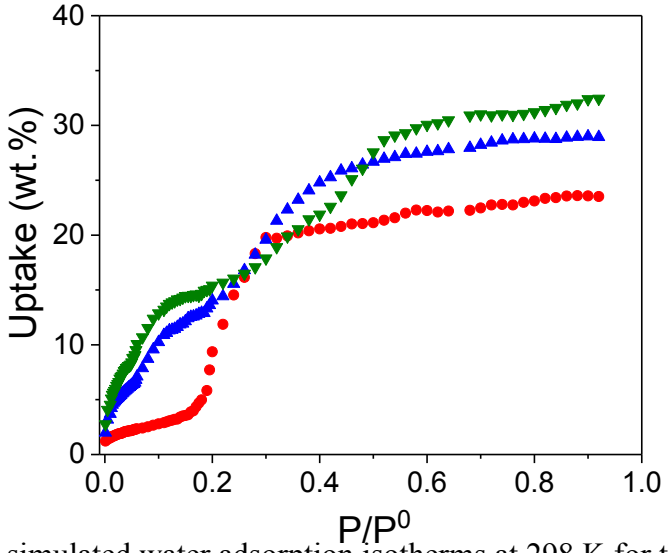

Figure S4. GCMC simulated water adsorption isotherms at 298 K for the linker defective ml_1 (●) configuration and the cluster defective mc_2 (▲), and mc_3 (▼) configurations with OH/H_2O as capping functions.

2. Experimental section

Synthesis procedures

In the experimental part of this work, two MOF-801 samples were prepared. The sample reported as 1 was prepared under solvothermal conditions using formic acid as a modulator while the sample reported as 2 was synthesized under hydrothermal conditions. Both samples followed preparation protocols reported in the literature[18,19]. The detailed description of the synthesis protocols is described below.

Synthesis of sample 1: $ZrOCl_2 \cdot 8H_2O$ (25.78 g, 80.0 mmol) and fumaric acid (9.286 g, 80.0 mmol) were dissolved in N,N-Dimehtylformaide (288 ml, 4.15 mol) and added formic acid (136.6 g, 2.968 mol) into a reaction solution. After stirring for 30 min at RT, the reaction solution was transferred to 1L Teflon-lined autoclave and heated 130 ^{o}C for 6 h. After cooling the reaction solution, the crystalline sample 1 were collected after purified with each three times for 500ml of DMF and MeOH by filteration.[18]

Synthesis of sample 2: $ZrCl_4$ (6.024 g, 25.85mmol) and Fumaric acid (8.995 g, 77.50 mmol) were dissolved in 500 ml of DI water and added formic acid (119 g, 2.585 mol) into a reaction solution. After stirring for 30min at RT, the reaction solution was transferred to a 1L Teflon-lined autoclave and heated 120 °C for 18 h. The crystalline sample 2 was recovered by centrifuge after purification with 500ml DI water and EtOH at RT for 3 h.[19]

*Structure and porosity characterization of MOF-801 samples **1** and **2**.*

Powder X-ray diffraction patterns of both samples were collected with a Rigaku D/MAX 2200/PC diffractometer using Ni-filtered CuKα-radiation (40 kV, 40 mA, λ=1.5406 Å) and a graphite crystal monochromator. The data was collected over the 2θ range from 5° to 50° for 4 sec in each 0.02° step scan at ambient temperature.

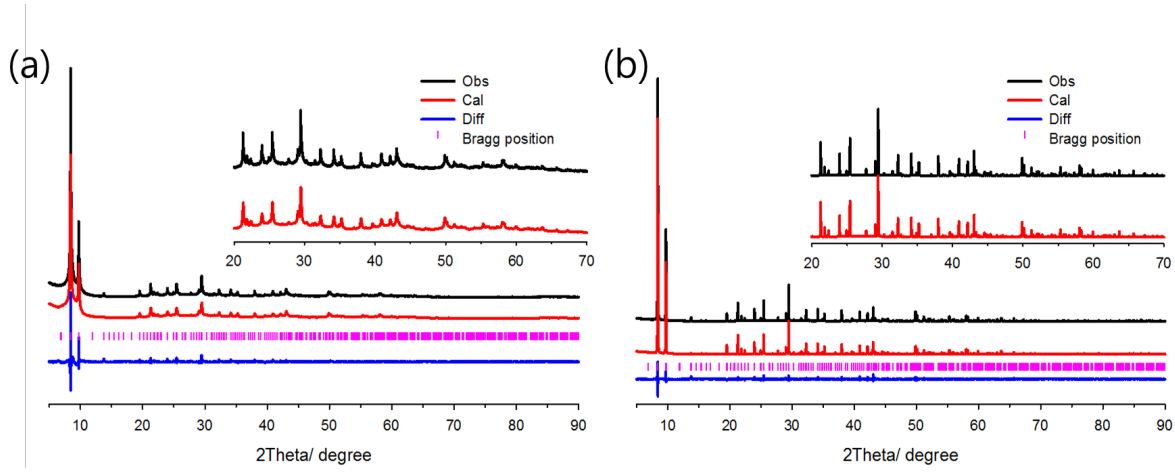

Figure S5. Rietveld refinement plot for (a) sample 1 and (b) sample 2. Tick marks i ndicate Bragg positions. For clarity, the plot has been magnified five times between 2 0 and 70°

For a detailed structural analysis of sample 1 and sample 2, synchrotron diffraction data were collected on beamline 9B at the Pohang Accelerator Laboratory (Pohang, Korea) using highly collimated monochromatic synchrotron radiation (λ=1.5167 Å). The detector arm of the vertical scan diffractometer consisted of seven sets of Soller slits, flat Ge(111) crystal analyzers, anti-scatter baffles, and scintillation detectors, with each set separated by 20°. Data were obtained on the sample at room temperature in flat-plate mode, with a step size of 0.01° for a scan time of 3s per step, and overlaps of 2° to the next detector bank over the 2θ range of 5–145°.

Diffraction patterns obtained were indexed using the DICVOL06 program implemented in the FullProf program suite. Profile refinement of the structure model 1 reported elsewhere including non-hydrogen atom only was performed using the Rietveld method in the JANA2006 package or the GSAS program package. During Rietveld refinement, a pseudo-Voigt function and microscopic broadening, together with a manually interpolated background, were used to describe the peak shapes. The fumarate was considered as rigid

body and its thermal motion was described using Translation-Libration-Screw (TLS) method.[20]

Table S1. Experimental data on Rietveld refinement of MOF-801 samples.

Material	Sample 1	Sample 2
Unit cell Composition	C24 O40.085 Zr6	C24 O42.457 Zr6
Refined structure		
Symmetry	cubic	cubic
space group	*P n -3*	*P n -3*
***a*, Å**	17.8920(16)	17.89982(18)
cell volume, Å^3	5727.6(9)	5735.17(10)
Wavelength/Å	1.5167	1.5167
Radiation type	Synchrotron Radiation	Synchrotron Radiation
No. Observation	1616	1622
No. Parameters	58	73
No. Restraints	4	4
No. Constraints	0	1
Max Change/s.u.	0.0673	0.0825
Largest Peak	0.99	1.91
Deepest Hole	-3.28	-2.27
R_p, %	5.67	8.78
R_{wp}, %	7.63	13.72
R_F, %	2.70	2.14
GOF	2.82	6.4

Scanning electron microscopy (SEM) images were analyzed by the Tescan Mira 3 LMU FEG at 10 kV acceleration voltage, and the samples were coated with Pt for 2 min after evacuation in the Quorum Q 150T ES equipment before analysis.

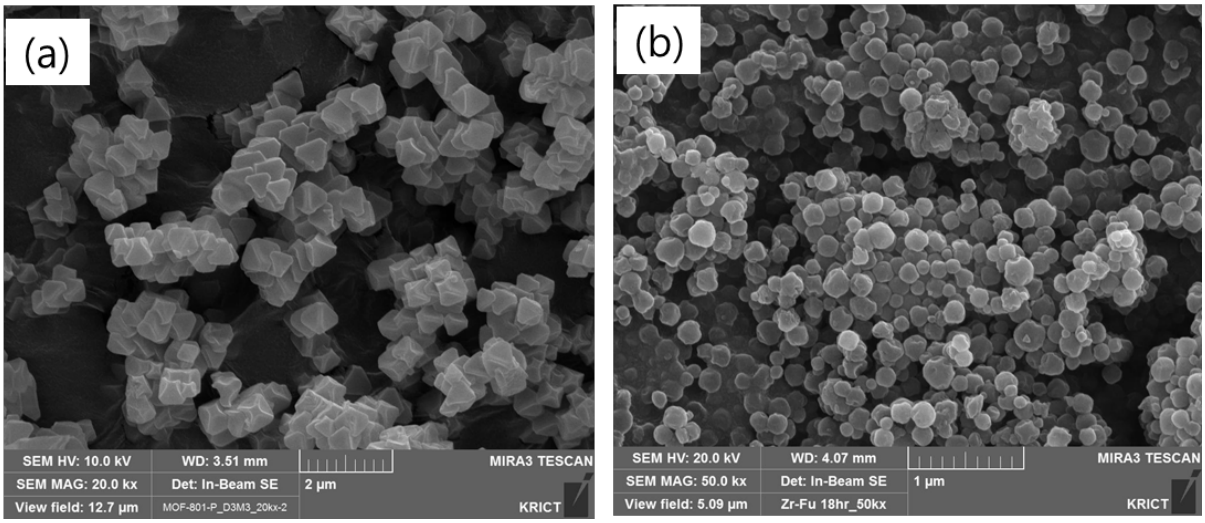

Figure S6. SEM images for MOF-801 sample 1 (a) and sample 2 (b).

Liquid-state H^1-NMR was performed on a Bruker Avance-700 FT-NMR Spectrometer after dissolving 50mg of sample into the mixture of 20 μl of 48 wt.% HF aqueous solution and 1 ml of DI water.

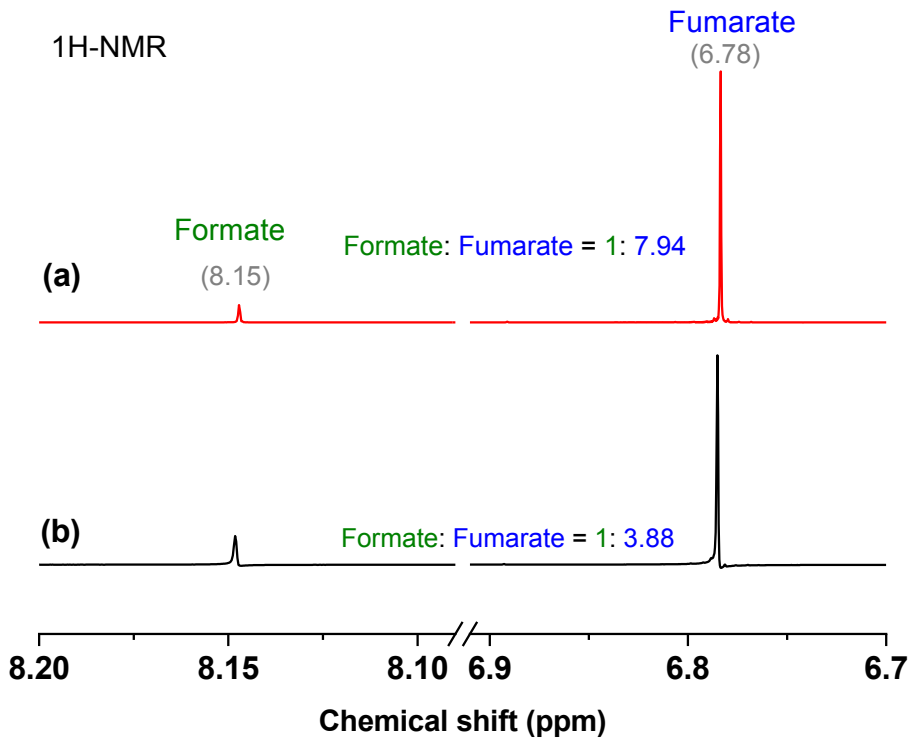

Figure S7. ^{1}H NMR spectra of MOF-801 sample 1 (a) and sample 2 (b)**.** The chemical shift of proton in formate was observed at 8.15ppm and that in fumarate was observed at 6.78 ppm. From the integrated proton area of each compound, the mole ratio of formate to fumarate were calculated.

Experimental quantification of defects.

Calculation of defect by TGA: Thermogravimetric analysis (TGA) was obtained with TA Instruments SDT-Q600 model under 100 ml/min Air flow with 5 °C/min of heating rate after dried sample at 100 °C (Figure S11a, b). And then, TG curve of y-axis are plotted by weight fraction on the basis of 100 wt % ZrO_2 assuming that residual weight fraction at 800°C is pure ZrO_2 after full decomposition of the fumarate linker (Figure S11 c, d). The theoretical non-defective MOF-801 framework have $Zr_6(\mu_3\text{-}O)_6(\text{fumarate})_6$ before started to decomposition of the coordinated fumarate linker, and the its wt % loss of fumarate linker per 100 wt % ZrO_2 is 79.59 wt %. From the comparison between experimental data and theoretical value of loss wt % of fumarate on the basis of ZrO_2 in each samples, the coordinated numbers of fumarate (x value) can be determined, which is followed to be calculation of the concentration of defect.[21,22]

$$x\ value = 6\times\frac{Weigt\ loss\ \%\ of\ furmate\ for\ defective\ MOF-801}{Weigt\ loss\ \%\ of\ furmate\ for\ non-defective\ MOF-801}$$

$$The\ concentration\ of\ defect = \frac{12-2x}{Molecular\ weight\ of\ non-defective\ MOF-801}$$

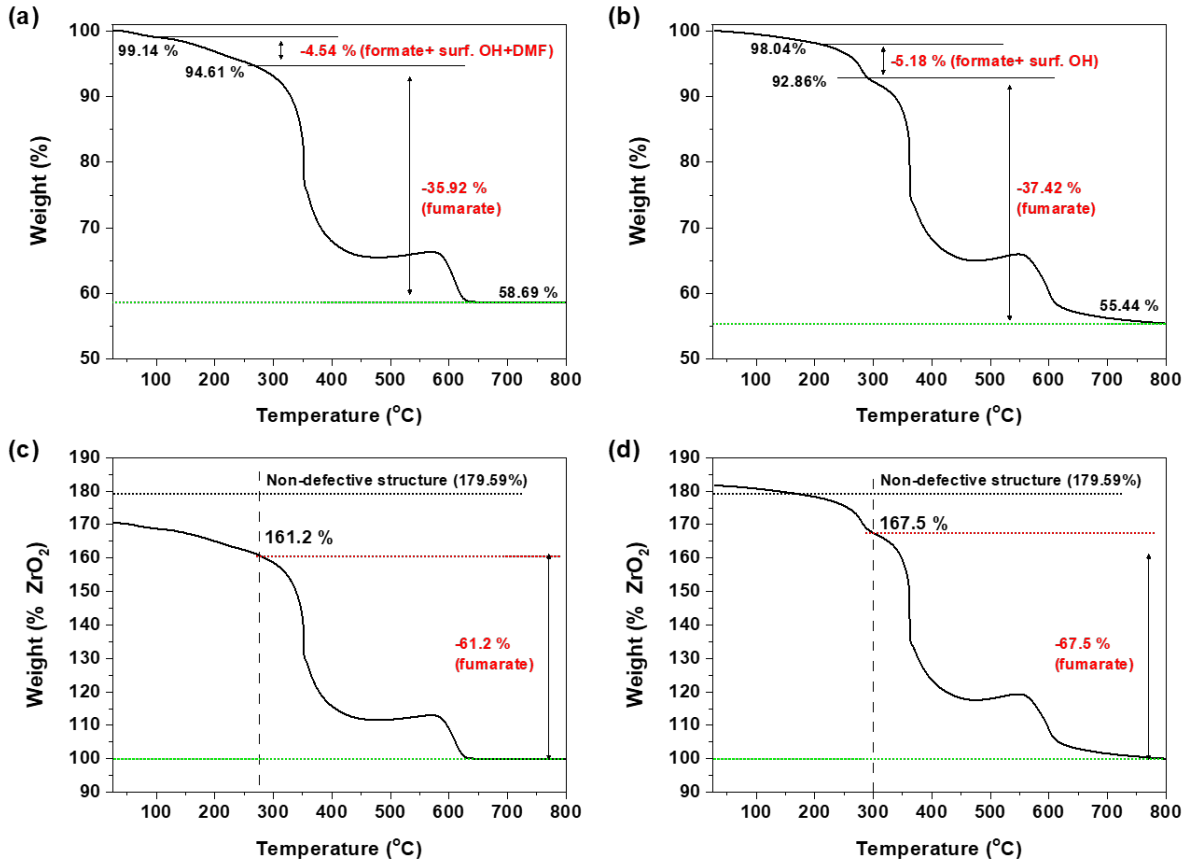

Figure S8. TGA results of samples after dried at 100 °C. (a) sample 1 and (b) sample 2 measured under 100ml/min Air flow with heating rate of 5 °C/min. TGA patterns plotted by the weight loss % per ZrO_2 for (c) sample 1 and (d) sample 2.

Calculation of defect by EA: The quantitative C, H, N elemental analysis for samples was determined using the Thermo Scientific FLASH 2000 series. From the EA data of carbon (C_{obs} wt%), hydrogen (H_{obs} wt%), and nitrogen weight fractions (N_{DMF} wt%), the carbon and hydrogen weight fractions were further calibrated by removing the weight fractions of carbon and hydrogen originated from residual DMF molecule in the framework because the value of carbon weigh fraction should only result in C_{obs} wt% of EA data from the coordinated fumarate organic linker and formate capping anion. The detection of nitrogen is only due to the residual DMF. Thus, the carbon weight fraction from DMF (C_{DMF} wt%) can

be determined from the weight fraction of nitrogen (N_{DMF} wt%) in EA data, and the calibrated carbon weight fraction (C_{calib} wt%) can be calculated by subtraction of C_{DMF} wt% from C_{obs} wt% using the following equation, where C_i *wt* and N_i *wt* correspond to the carbon weight and nitrogen weight per 1 mole of *i* molecule.

$$C_{\text{calib}}\ \text{wt\%} = C_{obs}\ wt\% - C_{DMF}\ wt\% = C_{obs}\ wt\% - N_{DMF}\ wt\% \times \frac{C_{DMF}\ wt}{N_{DMF}\ wt}$$

After calibration of C_{obs} wt% to C_{calib} wt% for both *Zr-Fumarate* MOFs, the carbon weight fractions of fumarate (C_{FUM} wt%) and formate (C_{FA} wt%) in EA data can be determined by using the experimental mole fraction (mol %) of fumarate (Mol_{FUM}) and formate (Mol_{FA}) obtained by 1H-NMR data.

$$Mol_{FUM\ or\ FA}(\%) = \frac{mole\ ratio\ of\ fumarate\ or\ formate}{sum\ of\ mole\ ratio\ for\ fumarate\ and\ formate} \times 100$$

$$C_{FUM\ or\ FA}\ wt\% = C_{calib}\ wt\% \times \frac{MOl_{Fum\ or\ FA} \times C_{FUM\ or\ FA}\ wt}{(MOl_{Fum} \times C_{Fum}\ wt + MOl_{FA} \times C_{FA}\ wt)}$$

The carbon weight fractions of fumarate and formate were converted to the weight fractions of fumarate (W_{FUM} wt%) and formate (W_{FA} wt%) from EA data.

$$W_{FUM}\ wt\% = C_{FUM\ or\ FA}\ wt\% \times \frac{Molecular\ Weight\ of\ Fumarate\ or\ Formate}{C_{FUM\ or\ FA}\ wt}$$

The concentration of defect can be calculated by comparing the theoretical formula for the dehydrated *Zr-Fumarate* MOF having $Zr_6(\mu_3\text{-}O)_4(\mu_3\text{-}OH)_4(\text{Fumarate})_6$. In this study, the coordinated formate is considered as defect site since this site is formed by the missing fumarate linker in the framework. The calculated value of W_{FUM} wt % is just observation value on the basis of $Zr_6(\mu_3\text{-}O)_4(\mu_3\text{-}OH)_4(\text{Fumarate})_a(\text{Formate})_b(\text{DMF})_c$. Hence, W_{FUM} wt% have to be recalculated on the basis of $Zr_6(\mu_3\text{-}O)_4(\mu_3\text{-}OH)_4(\text{Fumarate})x$.

$$W_{FUM,Calib}\ wt\% = W_{FUM}\ wt\% \times \frac{100}{100 - W_{FA}\ wt\% - W_{DMF}\ wt\%}$$

$$W_{DMF}\ wt\% = N_{DMF}\ wt\ \% \times \frac{Molecular\ weigh\ of\ DMF}{N_{DMF}\ wt}$$

The coordination numbers of fumarate (x value) and the concentration of defects (mmol g^{-1} MOF) in each samples can be determined by comparing the theoretical weight fraction of non-defective Zr-Fumarate MOF (50.19 wt% of $W_{\text{FUM, Theoretical}}$ wt%). Two defect sites are generated per one missing fumarate linker on the basis of Zr_6 cluster, which can be coordinated to 12 carboxylate groups.

$$\text{x} = 6 \times \frac{W_{FUM,Calib}\ wt\%}{W_{FUM,Theoretical}\ wt\%}$$

$$The\ concentration\ of\ defect = \frac{12 - 2x}{Molecular\ weight\ of\ Zr - Fumarate\ MOF}$$

The structural formula of $Zr_6(\mu_3\text{-}O)_4(\mu_3\text{-}OH)_4(\text{Fumarate})_x(\text{Formate})_y(\text{OH-}H_2O\ \text{pair})_z$ for each samples can be determined by using the molar ratio (fumarate/formate) from 1H-NMR data, and the defect site capping with OH/H_2O pair (z value) also calculated by charge balance of framework.

$$The\ coordination\ number\ of\ formate\ (y\ value) = x\ value \times molar\ ratio\ (formate/fumarate)$$

$$The\ coordination\ number\ of\ OH/H2O\ pair\ (z\ value) = 12 - 2x - y$$

From the calculation of combined method by EA and 1H-NMR, we determined the dehydrated structure formula of each sample as reported in **Table S2.**

Table S2. Chemical formula of Zr-Fumarate MOFs calculated by combining EA and ^{1}H NMR experimental data

Sample	Structure formula of dehydrated *Zr-Fumarate* MOFs	Molar ratio (Fumarate / Formate)	Molar ratio (OH/H_2O pair/ Formate)
Sample 1	$Zr_6(O)_4(OH)_4(Fumarate)_{4.745}(Formate)_{0.598}(OH/H_2O)_{1.912}$	7.94	3.20
Sample 2	$Zr_6(O)_4(OH)_4(Fumarate)_{5.095}(Formate)_{1.313}(OH/H_2O)_{0.497}$	3.88	0.38

To determine the porosity of the samples, N_2 isotherms were measured with a Micromeritics Tristar 3020 at 77 K after they have been activated at 150 °C for 12 h under ~10^{-5} torr vacuum conditions. The BET area (S_{BET}) was calculated using the Brunauer-Emmett-Teller (BET) method, and total pore volume (V_p) was taken by a single point method at $P/P^0 = 0.99$. Additionally, the micropore surface area (S_{micro}) and the pore volume ($V_{p,micro}$) were determined using the t-plot method. To obtain the pore size distribution of two samples, Ar isotherm was conducted under liquid Ar temperature (87K) by using ASAP 2020 equipment.

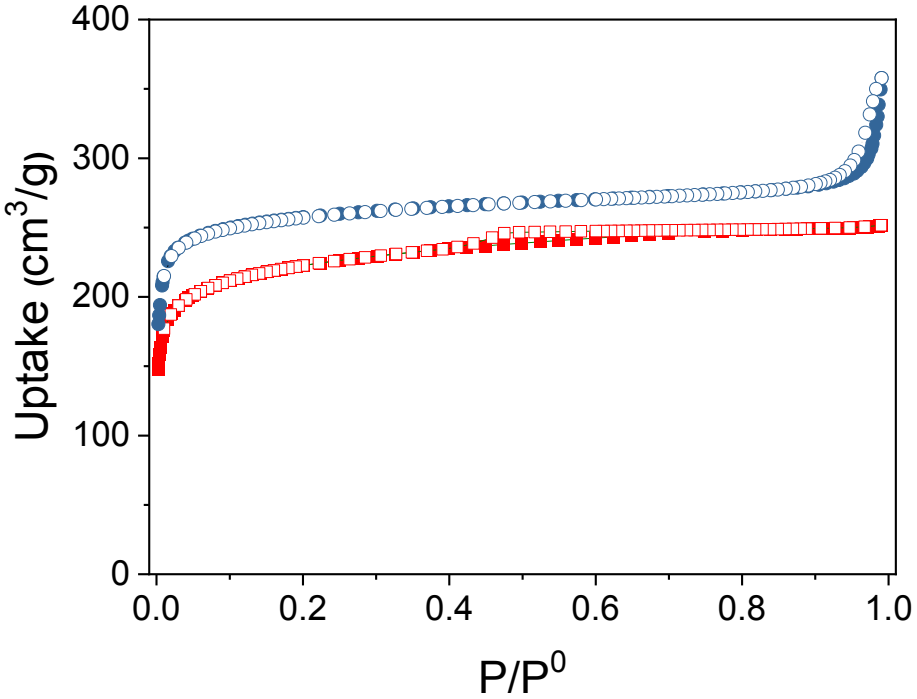

Figure S9. N_2 adsorption (filled symbols) and desorption (empty symbols) isotherms of the MOF-801 samples **1** (red squares) and **2** (blue circles) at 77K.

Table S2. Textural characteristics of MOF-801 sample 1 and sample 2.

Sample	S_{BET} (m^2/g)	S_{micro} (m^2/g)	$V_{p,total}$ (cm^3/g)	$V_{p,micro}$ (cm^3/g)
Sample 1	840	765	0.389	0.320
Sample 2	1026	977	0.553	0.382

Pore size distribution (PSD) plots were fitted from Ar isotherms at 87 K of the MOF-801 sample 1 and sample 2 measured in the micromeritics ASAP 2020_Ar at 87K_oxide model using non-linear density function theory (NLDFT). Such pore size distributions were compared with the PSDs obtained from structure models used to represent both experimental samples.

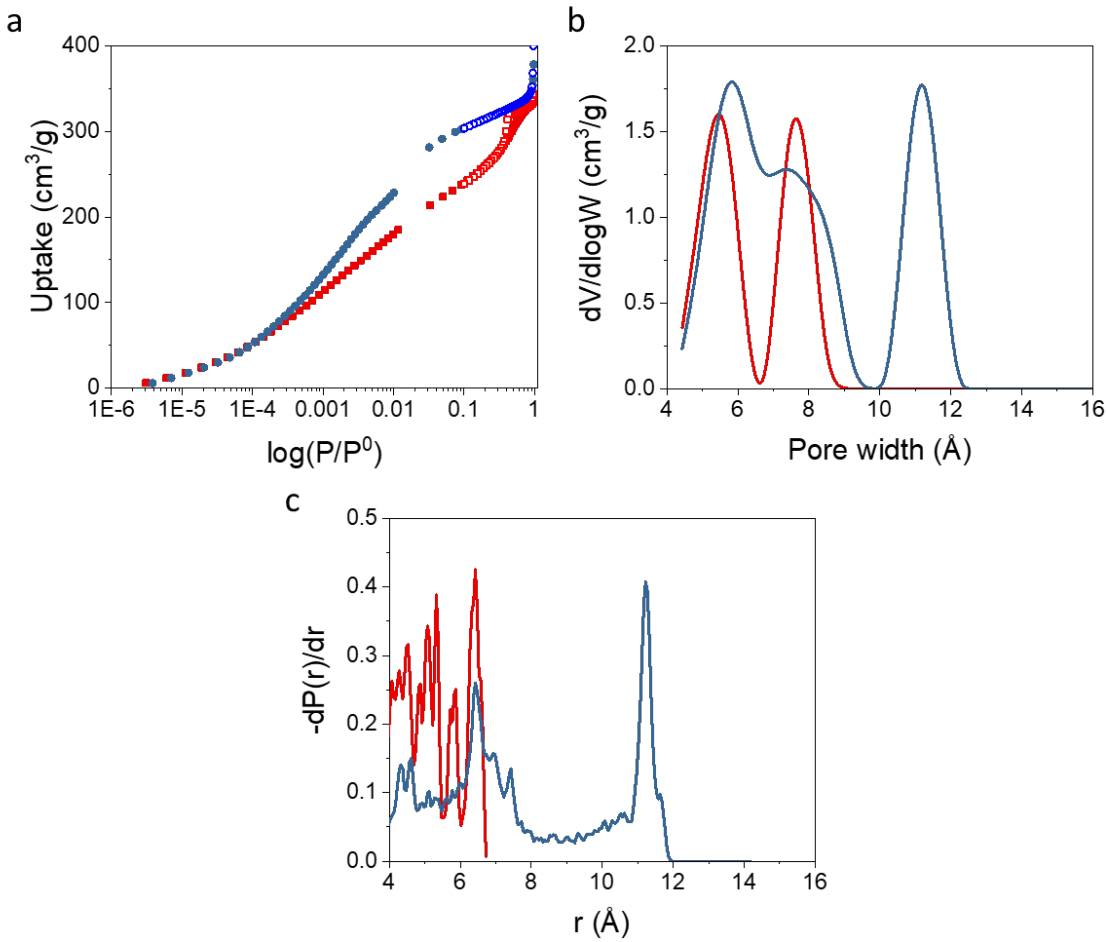

Figure S10. (a) Argon adsorption (filled symbols) and desorption (empty symbols) isotherms measured at 87 K from the MOF-801 samples **1** (red squares) and **2** (blue circles). (b) Pore size distributions (PSDs) of samples **1** (red line) and **2** (blue line) obtained by NLDFT fitting of the Ar experimental isotherms. (c) Pore size distributions calculated from structure models **1** (red line) and **2** (blue line).

Water sorption measurements.

Water sorption isotherms and test for adsorptive chiller have been measured by an intelligent gravimetric analyser (IGA, Hiden Analytical Ltd.). The IGA was automatically operated to precisely control the water vapour pressure (1-95% RH) and temperature (20-100 $^{\circ}$C). Prior to adsorption experiments, samples were dehydrated at 100 $^{\circ}$C for 1h under high vacuum ($<10^{-6}$ Torr).

References

(1) Choi, J.; Lin, L.-C.; Grossman, J. C. Role of Structural Defects in the Water Adsorption Properties of MOF-801. *J. Phys. Chem. C* **2018**, *122* (10), 5545–5552. https://doi.org/10.1021/acs.jpcc.8b00014.

(2) Perdew, J. P.; Burke, K.; Ernzerhof, M. Generalized Gradient Approximation Made Simple. *Phys. Rev. Lett.* **1996**, *77* (18), 3865–3868. https://doi.org/10.1103/PhysRevLett.77.3865.

(3) Hutter, J.; Iannuzzi, M.; Schiffmann, F.; VandeVondele, J. <scp>cp2k:</Scp> Atomistic Simulations of Condensed Matter Systems. *Wiley Interdiscip. Rev. Comput. Mol. Sci.* **2014**, *4* (1), 15–25. https://doi.org/10.1002/wcms.1159.

(4) VandeVondele, J.; Krack, M.; Mohamed, F.; Parrinello, M.; Chassaing, T.; Hutter, J. Quickstep: Fast and Accurate Density Functional Calculations Using a Mixed Gaussian and Plane Waves Approach. *Comput. Phys. Commun.* **2005**, *167* (2), 103–128. https://doi.org/10.1016/j.cpc.2004.12.014.

(5) Weigend, F.; Ahlrichs, R. Balanced Basis Sets of Split Valence, Triple Zeta Valence and Quadruple Zeta Valence Quality for H to Rn: Design and Assessment of Accuracy. *Phys. Chem. Chem. Phys.* **2005**, *7* (18), 3297. https://doi.org/10.1039/b508541a.

(6) Krack, M. Pseudopotentials for H to Kr Optimized for Gradient-Corrected Exchange-Correlation Functionals. *Theor. Chem. Acc.* **2005**, *114* (1–3), 145–152. https://doi.org/10.1007/s00214-005-0655-y.

(7) Goedecker, S.; Teter, M.; Hutter, J. Separable Dual-Space Gaussian Pseudopotentials. *Phys. Rev. B* **1996**, *54* (3), 1703–1710. https://doi.org/10.1103/PhysRevB.54.1703.

(8) Grimme, S.; Antony, J.; Ehrlich, S.; Krieg, H. A Consistent and Accurate Ab Initio Parametrization of Density Functional Dispersion Correction (DFT-D) for the 94 Elements H-Pu. *J. Chem. Phys.* **2010**, *132* (15), 154104. https://doi.org/10.1063/1.3382344.

(9) Campañá, C.; Mussard, B.; Woo, T. K.; Campañá, C.; Mussard, B.; Woo, T. K. Electrostatic Potential Derived Atomic Charges for Periodic Systems Using a Modified Error Functional. *J. Chem. Theory Comput.* **2009**, *5* (10), 2866–2878. https://doi.org/10.1021/ct9003405.

(10) Vlugt, T. J. H.; García-Pérez, E.; Dubbeldam, D.; Ban, S.; Calero, S. Computing the Heat of Adsorption Using Molecular Simulations: The Effect of Strong Coulombic Interactions. *J. Chem. Theory Comput.* **2008**, *4* (7), 1107–1118. https://doi.org/10.1021/ct700342k.

(11) Rappé, A. K. K.; Casewit, C. J. J.; Colwell, K. S. S.; Goddard III, W. A.; Skiff, W. M. M.; Rappe, A. K.; Casewit, C. J. J.; Colwell, K. S. S.; Goddard, W. A.; Skiff, W. M. M. UFF, a Full Periodic Table Force Field for Molecular Mechanics and Molecular Dynamics Simulations. *J. Am. Chem. Soc.* **1992**, *114* (25), 10024–10035. https://doi.org/10.1021/ja00051a040.

(12) Mayo, S. L.; Olafson, B. D.; Iii, W. a G.; Eb, E.; El, E. a E. T. DREIDING: A Generic Force Field for Molecular Simulations. *J. Phys. Chem.* **1990**, *101* (Suite 540), 8897–8909. https://doi.org/10.1021/j100389a010.

(13) Lorentz, H. A. Ueber Die Anwendung Des Satzes Vom Virial in Der Kinetischen Theorie Der Gase. *Ann. Phys.* **1881**, *248* (1), 127–136. https://doi.org/10.1002/andp.18812480110.

(14) Ewald, P. P. Die Berechnung Optischer Und Elektrostatischer Gitterpotentiale. *Ann. Phys.* **1921**, *369* (3), 253–287. https://doi.org/10.1002/andp.19213690304.

(15) Jorgensen, W. L.; Maxwell, D. S.; Tirado-Rives, J. Development and Testing of the OPLS All-Atom Force Field on Conformational Energetics and Properties of Organic Liquids. *J. Am. Chem. Soc.* **1996**, *118* (45), 11225–11236. https://doi.org/10.1021/ja9621760.

(16) Wick, C. D.; Stubbs, J. M.; Rai, N.; Siepmann, J. I. Transferable Potentials for Phase Equilibria. 7. Primary, Secondary, and Tertiary Amines, Nitroalkanes and Nitrobenzene, Nitriles, Amides, Pyridine, and Pyrimidine. *J. Phys. Chem. B* **2005**, *109* (40), 18974–18982. https://doi.org/10.1021/jp0504827.

(17) Abascal, J. L.; Vega, C. A General Purpose Model for the Condensed Phases of Water: TIP4P/2005. *J. Chem. Phys.* **2005**, *123* (23), 234505. https://doi.org/10.1063/1.2121687.

(18) Furukawa, H.; Gándara, F.; Zhang, Y.-B.; Jiang, J.; Queen, W. L.; Hudson, M. R.; Yaghi, O. M. Water Adsorption in Porous Metal–Organic Frameworks and Related Materials. *J. Am. Chem. Soc.* **2014**, *136* (11), 4369–4381. https://doi.org/10.1021/ja500330a.

(19) Zahn, G.; Schulze, H. A.; Lippke, J.; König, S.; Sazama, U.; Fröba, M.; Behrens, P. A Water-Born Zr-Based Porous Coordination Polymer: Modulated Synthesis of Zr-Fumarate MOF. *Microporous Mesoporous Mater.* **2015**, *203*, 186–194. https://doi.org/10.1016/j.micromeso.2014.10.034.

(20) Dunitz, J. D.; Schomaker, V.; Trueblood, K. N. Interpretation of Atomic Displacement Parameters from Diffraction Studies of Crystals. *J. Phys. Chem.* **1988**, *92* (4), 856–867. https://doi.org/10.1021/j100315a002.

(21) Katz, M. J.; Brown, Z. J.; Colón, Y. J.; Siu, P. W.; Scheidt, K. A.; Snurr, R. Q.; Hupp, J. T.; Farha, O. K. A Facile Synthesis of UiO-66, UiO-67 and Their Derivatives. *Chem. Commun.* **2013**, *49* (82), 9449–9451. https://doi.org/10.1039/c3cc46105j.

(22) Shearer, G. C.; Chavan, S.; Ethiraj, J.; Vitillo, J. G.; Svelle, S.; Olsbye, U.; Lamberti, C.; Bordiga, S.; Lillerud, K. P. Tuned to Perfection: Ironing Out the Defects in Metal − Organic Framework UiO-66. **2014**, 13–16. https://doi.org/10.1021/cm501859p.